

UniRGB-IR: A Unified Framework for Visible-Infrared Semantic Tasks via Adapter Tuning

Maoxun Yuan*
Institute of Artificial Intelligence,
Beihang University
Beijing, China

Bo Cui*
School of Computer Science and
Engineering, Beihang University
Beijing, China

Tianyi Zhao
Institute of Artificial Intelligence,
Beihang University
Beijing, China

Jiayi Wang
China Academy of Information and
Communications Technology
Beijing, China

Shan Fu
China Academy of Information and
Communications Technology
Beijing, China

Xue Yang
Shanghai Jiao Tong University
Shanghai, China

Xingxing Wei[†]
Institute of Artificial Intelligence,
Beihang University
Beijing, China

Abstract

Semantic analysis on visible (RGB) and infrared (IR) images has gained significant attention due to their enhanced accuracy and robustness under challenging conditions including low-illumination and adverse weather. However, due to the lack of pre-trained foundation models on the large-scale infrared image datasets, existing methods prefer to design task-specific frameworks and directly fine-tune them with pre-trained foundation models on their RGB-IR semantic relevance datasets, which results in poor scalability and limited generalization. To address these limitations, we propose **UniRGB-IR**, a scalable and efficient framework for RGB-IR semantic tasks that introduces a novel adapter mechanism to effectively incorporate rich multi-modal features into pre-trained RGB-based foundation models. Our framework comprises three key components: a vision transformer (ViT) foundation model, a Multi-modal Feature Pool (MFP) module, and a Supplementary Feature Injector (SFI) module. The MFP and SFI modules cooperate with each other as an adapter to effectively complement the ViT features with the contextual multi-scale features. During training process, we freeze the entire foundation model to inherit prior knowledge and only optimize the MFP and SFI modules. Furthermore, to verify the effectiveness of our framework, we utilize the ViT-Base as the pre-trained foundation model to perform extensive experiments. Experimental results on various RGB-IR semantic tasks demonstrate

that our method can achieve state-of-the-art performance. The code is available at <https://github.com/PoTtsui99/UniRGB-IR.git>.

CCS Concepts

• **Computing methodologies** → **Object detection; Image segmentation; Scene understanding.**

Keywords

RGB-IR semantic tasks, multi-modal fusion, adapter

ACM Reference Format:

Maoxun Yuan, Bo Cui, Tianyi Zhao, Jiayi Wang, Shan Fu, Xue Yang, and Xingxing Wei. 2025. UniRGB-IR: A Unified Framework for Visible-Infrared Semantic Tasks via Adapter Tuning. In . ACM, New York, NY, USA, 11 pages. <https://doi.org/XXXXXXXX.XXXXXXX>

1 Introduction

Image semantic analysis in the visible images is a common practice in computer vision and has been widely used in a variety of vision tasks such as object detection [2, 67], instance segmentation [24, 90], and semantic segmentation [60]. However, visible cameras have demonstrated significant limitations in providing reliable imaging [66, 72], due to their restricted spectral bandwidth. This constraint becomes particularly problematic under low-illumination conditions and adverse weather scenarios. Therefore, infrared (IR) imaging, with its superior low-light adaptability, has been increasingly employed as complementary information to enhance visible modality performance [66, 83]. Afterwards, the joint use of RGB and IR images has been applied in more and more semantic analysis tasks.

With the rapid advancements in physical computing capabilities, more and more general-purpose foundation backbones [10, 65] pre-trained on large-scale RGB-based datasets (e.g., ImageNet [9] and COCO [34]) have been designed for various tasks. Since these pre-trained models implicitly encode substantial prior knowledge, it is believed that pre-trained models can promote the improvement of downstream task performance and speed up training convergence. Therefore, fine-tuning the pre-trained foundation models [46, 61] on

*Equal Contribution.

[†]Corresponding Author.

Permission to make digital or hard copies of all or part of this work for personal or classroom use is granted without fee provided that copies are not made or distributed for profit or commercial advantage and that copies bear this notice and the full citation on the first page. Copyrights for components of this work owned by others than the author(s) must be honored. Abstracting with credit is permitted. To copy otherwise, or republish, to post on servers or to redistribute to lists, requires prior specific permission and/or a fee. Request permissions from permissions@acm.org.
Conference'17, Washington, DC, USA

© 2025 Copyright held by the owner/author(s). Publication rights licensed to ACM.
ACM ISBN 978-x-xxxx-xxxx-x/YYYY/MM
<https://doi.org/XXXXXXXX.XXXXXXX>

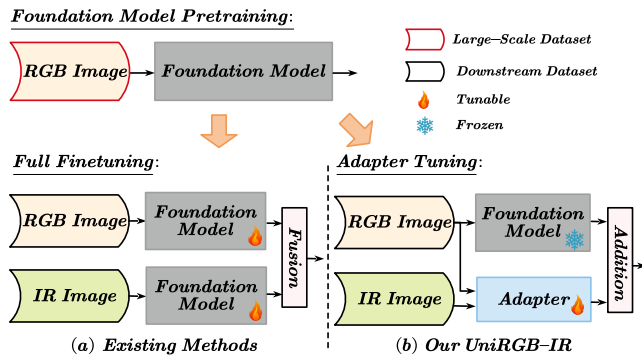


Figure 1: Existing full fine-tuning methods vs. our UniRGB-IR framework. (a) Existing methods use pre-trained RGB-based foundation models and fully fine-tune them on their RGB-IR semantic relevance datasets. (b) We utilize the Adapter [18] to propose a unified framework, which can efficiently introduce richer RGB-IR features into the pre-trained foundation model for various semantic tasks.

their semantic relevance datasets has become a common paradigm to improve the performance on downstream tasks.

However, due to the lack of pre-trained foundation models on the large-scale infrared image datasets, for RGB-Infrared semantic tasks, a straightforward and prevailing way [36, 77] is to use pre-trained RGB-based models and fine-tune them on their RGB-IR semantic relevance datasets as shown in Figure 1 (a). For example, RGB-IR object detectors [71, 77] utilize RGB-based models as strong baselines and fine-tune them to extract RGB and IR features. SwinNet [40] employs transformer architecture to extract hierarchical features across RGB and infrared modalities, effectively detecting salient RGB-IR objects. Similarly, Ha *et al.* [15] establish a novel baseline by incorporating infrared modality features into an RGB-based framework and fine-tune it on the RGB-IR semantic segmentation benchmark. Among the efforts to achieve competitive results, these approaches still suffer from two major issues:

❶ **Limited model versatility and redundant parameter storage.** Due to the lack of a unified framework for RGB-IR semantic tasks, different semantic tasks often require customized model structures tailored to specific objectives. However, task-specific customization often leads to poor model versatility, as each task demands its own dedicated model structure. Besides, maintaining multiple specialized models for different downstream tasks results in excessive parameter storage requirements.

❷ **Impairment of prior knowledge encoded in foundation models.** Pre-trained foundation models are typically initialized using large-scale datasets, where they learn rich feature representations that capture general visual patterns. However, the full fine-tuning strategy indiscriminately updates the model parameters to adapt to the task-specific RGB-IR datasets, which often overrides the prior knowledge encoded in the pre-trained model. This will reduce the generalization potential of the fine-tuned model.

Above challenges necessitate the adaptation of RGB-based foundation models to construct a unified framework capable of handling RGB-IR semantic tasks effectively.

Drawing inspiration from recent advances in adapters [18, 48], which are initially used to yield an extensible model to effectively

exploit the potential representation of foundation models in the natural language processing (NLP) field, we develop an adapter to dynamically introduce extensive RGB-IR features into the pre-trained RGB-based foundation model. In our adapter, a feature extractor is designed to obtain rich RGB-IR features and a feature injector is proposed to adaptively introduce the required features for the foundation model. Without altering the original RGB-based foundation model, the robust pre-trained weights can be directly preserved to expedite training convergence and enable efficient fine-tuning for downstream tasks. Consequently, in this paper, we establish a **Unified** framework for **RGB-IR** semantic tasks, termed **UniRGB-IR**, as illustrated in Figure 1 (b).

Specifically, we design two core modules in our UniRGB-IR: a **Multi-modal Feature Pool** module (MFP) and a **Supplementary Feature Injector** module (SFI). For the MFP module, the multi-receptive field convolution and the feature pyramid are deployed to capture contextual multi-scale features from RGB and IR images. These features are fused at different scales to complement foundation models for different RGB-IR semantic tasks. As for the SFI module, we implement a cross-attention mechanism that dynamically injects essential features into the pre-trained foundation model, endowing our UniRGB-IR framework with robust feature representation capabilities. To inherit prior knowledge of the foundation model pre-trained on the large-scale datasets, we utilize the adapter tuning paradigm instead of the full fine-tuning manner. We freeze the pre-trained weights and only optimize the adapter. Consequently, our UniRGB-IR can serve as a unified framework to achieve effective fine-tuning for various RGB-IR semantic tasks.

Overall, our contributions are summarized as follows:

- We explore an scalable and efficient framework called UniRGB-IR for RGB-IR semantic tasks. To the best of our knowledge, this is the first attempt to construct a unified framework for various RGB-IR downstream tasks.
- We design a Multi-modal Feature Pool module alongside a Supplementary Feature Injector module. The former extracts contextual multi-scale features from two modality images, and the latter dynamically injects the required features into the pre-trained model. These two modules can be efficiently fine-tuned with adapter tuning paradigm to complement the pre-trained foundation model with richer RGB-IR features for specific semantic task.
- We incorporate the vision transformer foundation model into the UniRGB-IR framework to evaluate the effectiveness of our method on RGB-IR semantic tasks, including RGB-IR object detection, RGB-IR semantic segmentation, and RGB-IR salient object detection. Extensive experimental results demonstrate that our methods can efficiently achieve superior performance on these downstream tasks.

2 Related Work

2.1 Vision Foundation Models

Recently, thanks to the powerful long-distance modeling capability, vision transformers (ViT) [10] have been widely used as the foundation model in many vision tasks to achieve competitive results. The original ViT is a plain, non-hierarchical structure for image classification. Based on it, ViTDet [31] also constructs a non-hierarchical

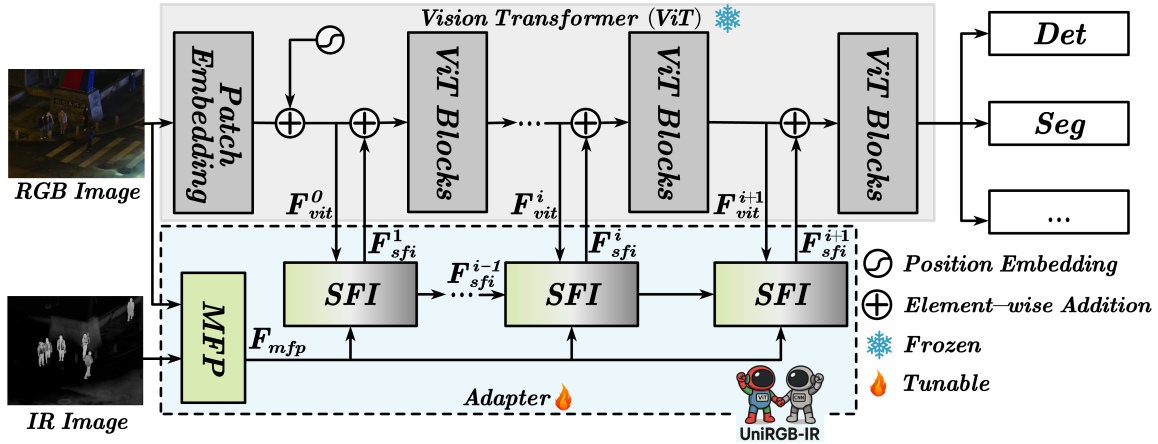


Figure 2: The overall architecture of our UniRGB-IR. In our framework, a ViT model with different numbers of ViT blocks is deployed as a foundation model, which is divided into N (usually $N = 4$) stages for feature interaction. During training, we freeze the entire ViT model weights and only optimize the MFP and SFI modules.

model by incorporating the feature pyramid. However, the non-hierarchical structure lacks rich feature representation, resulting in unsatisfactory performance. Subsequently, various hierarchical transformers [11, 28, 39, 65] have been proposed for different downstream vision tasks. Swin Transformer [39] and Multiscale Vision Transformer [11] are designed based on the ViT model to explore multi-scale features to improve the performance of image classification and object detection tasks. Besides, PVT [58] performs global attention on the downsampled key and value maps for dense prediction. In our work, we leverage the ViT model as our pre-trained foundation to build a unified framework for RGB-IR semantic tasks.

2.2 RGB-IR Semantic Tasks

RGB-IR Object Detection. Zhang *et al.* [76] explore a two-stream SSD [38] structure to capture the contextual enhanced features for RGB-IR object detection. Besides, AR-CNN [78] is presented based on Faster R-CNN [44] to align RGB and IR features. With the emergence of transformers, Yuan *et al.* [70] propose a complementary fusion transformer (CFT) module to achieve advanced detection results. Furthermore, C²Former [72] is a novel transformer block and can be incorporated into existed pre-trained models to increase intra- and inter-modality feature representations.

RGB-IR Semantic Segmentation. MFNet [15] is proposed to incorporate infrared features into the RGB-based framework to perform RGB-IR semantic segmentation. Based on the transformer structure, Wu *et al.* [63] propose a novel CCFNet to excavate discriminative and complementary modality features for RGB-IR semantic segmentation. Moreover, CMX [75] is designed as a universal cross-modal fusion framework for RGB-IR semantic segmentation in an interactive fusion manner.

RGB-IR Salient Object Detection. SwinNet [40] is designed based on the Swin Transformer to extract hierarchical information of each modality, which achieves impressive results. CAVER [42] introduces the transformer to rethink the bi-modal salient object detection from a sequence-to-sequence perspective, which increases the model interpretability. Recently, Zhou *et al.* [87] transfer a large

amount of knowledge learned in the transformer-based network to lightweight WaveNet through the distillation method.

The above methods attempt to design task-oriented structures to improve performance on corresponding downstream tasks. They either train the designed model from scratch or adopt a full fine-tuning strategy on a pre-trained model. Unlike these methods, we deploy an adapter based on the pre-trained foundation model for various RGB-IR semantic tasks.

2.3 Adapters

In the NLP field, Adapter [18] first fixes the original foundation backbone and introduces new modules into the transformer for task-specific fine-tuning, thereby effectively adapting the pre-trained backbone to downstream NLP tasks. Afterwards, Adapter has been widely studied in computer vision. ViT-Adapter [8], Low-Rank Adapter [69] and Mona [68] are designed to introduce a modest number of trainable parameters into the ViT and fine-tuning efficiently for dense prediction tasks. In addition, PC-Adapter [43] explores an attention-based adapter to preserve global shape knowledge for domain adaptation on point cloud data. Recently, Adapter is also used as a parameter-efficient training technology for vision-and-language tasks [50, 55].

In this paper, we aim to explore an adapter capable of converting the IR features into the RGB features to fit the pre-trained foundation model, which remains a challenge to design this unified framework. Our UniRGB-IR is the first to propose utilizing adapter for RGB-IR semantic tasks.

3 Method

3.1 Overall Architecture

The overall framework of UniRGB-IR is illustrated in Figure 2, which consists of three parts: vision transformer model, Multi-modal Feature Pool (MFP) module, and Supplementary Feature Injector (SFI) module. In our framework, the ViT model is utilized as the pre-trained foundation model and frozen during the training process. Specifically, for the ViT model, the RGB image is directly fed into

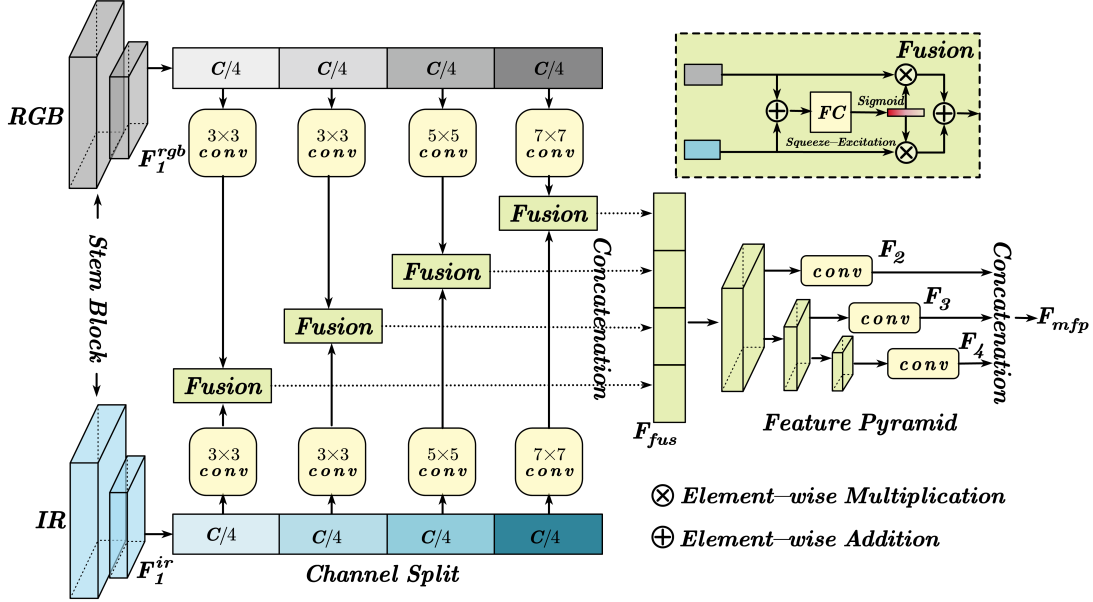


Figure 3: Structure of the multi-modal feature pool (MFP) module. We explore multiple perceptions to expand the receptive field of contextual feature extraction and utilize the feature pyramid to obtain the multi-scale features.

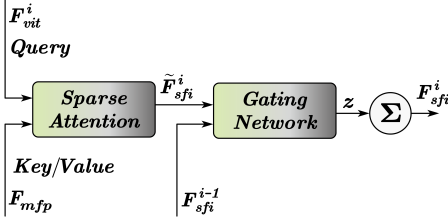


Figure 4: Structure of supplementary feature injector (SFI) module. A gating network is utilized to dynamically fuse the current and the last injected features.

the patch embedding process to obtain the D -dimensional feature tokens, which are usually $1/16$ of the original image resolution. To complement the richer features required for various RGB-IR semantic tasks, we feed the RGB and IR images into the MFP module to extract contextual multi-scale features from two modalities (eg. $1/8$, $1/16$ and $1/32$ of the original image resolution). Afterwards, these richer features are dynamically injected into the features of ViT model through the SFI module, which can adaptively introduce the required RGB-IR features into the ViT model. To fully integrate the extracted features into the ViT model, we add the SFI module at the beginning of each stage. Consequently, after N stages of feature injection, the final features from ViT model can be leveraged for various RGB-IR semantic tasks.

3.2 Multi-modal Feature Pool

To complement the rich feature representations for RGB-IR semantic tasks, we introduce a multi-modal feature pool (MFP) module, including multiple perception and feature pyramid. The former can extract the contextual features with different convolution kernels, which achieve the long-distance modeling capability of CNNs. Different from existing works [17, 64] that increase the width or

depth of the model, we efficiently achieve multi-receptive field perception in the channel dimension. As for feature pyramid, it can obtain multi-scale features to enhance the small object features. Thus, these two operations are connected in series to construct MFP module, as shown in Figure 3.

Specifically, for the input RGB ($H \times W \times 3$) and IR ($H \times W$) images, we first employ a stem block borrowed from ResNet [16] to extract two modality features F_1^{rgb} and $F_1^{ir} \in \mathbb{R}^{H/4 \times W/4 \times C}$. Then, these two features are split into four equal parts by utilizing channel splitting. To extract multi-receptive field perception, each part is subjected to convolution operations with different kernel sizes (3×3 , 3×3 , 5×5 and 7×7). Then, we fuse each processed feature from two modalities by using SE attention [19] (shown in Figure 3). Therefore, we concatenate each fused part to obtain RGB-IR contextual features F_{fus} , which can be formulated as:

$$F_{fus} = \Gamma_{k=1}^4 (Fus(W_k^{rgb} * f_k^{rgb}, W_k^{ir} * f_k^{ir})), \quad (1)$$

where $F_{fus} \in \mathbb{R}^{H/4 \times W/4 \times C}$, f_k^{rgb} and f_k^{ir} are the k -th part of F_1^{rgb} and F_1^{ir} features respectively, W_k is the convolution with k -th kernel size, Γ is the concatenation operation, $Fus(\cdot, \cdot)$ denotes the fusion module as shown in Figure 3.

For the feature pyramid, a stack of three 3×3 convolutions with $stride = 2$ is applied to downsample the size of the feature maps. Then, features of each scale are fed into a 1×1 convolution to project the feature maps to D dimensions. Therefore, we can obtain a set of multi-scale features $\{F_2, F_3, F_4\}$ with $1/8$, $1/16$, and $1/32$ of the original image resolution, respectively. Finally, we flatten and concatenate these features into feature tokens $F_{mfp} \in \mathbb{R}^{(\frac{HW}{8^2} + \frac{HW}{16^2} + \frac{HW}{32^2}) \times D}$, which will be used as supplementary features for the ViT foundation model.

Table 1: RGB-IR object detection results (mAP, in%) on the FLIR and LLVIP dataset. The best results are highlighted in red and the second-best are highlighted in blue. “-” indicates that the authors do not provide the corresponding results.

Methods	Modality	FLIR			LLVIP		
		mAP	mAP ₅₀	mAP ₇₅	mAP	mAP ₅₀	mAP ₇₅
SSD [38]	IR	24.6	57.0	18.0	53.5	90.2	57.9
RetinaNet [33]	IR	31.5	66.1	25.3	55.1	94.8	57.6
Faster R-CNN [44]	IR	37.6	75.8	31.6	54.5	94.6	57.6
Cascade R-CNN (ViT-B) [3]	IR	41.9	78.6	37.3	60.4	94.9	67.5
DDQ-DETR [80]	IR	37.1	73.9	32.2	58.6	93.9	64.6
SSD [38]	RGB	18.8	46.3	13.1	39.8	82.6	31.8
RetinaNet [33]	RGB	21.9	51.2	15.2	42.8	88.0	34.4
Faster R-CNN [44]	RGB	27.7	62.2	21.2	45.1	87.0	41.2
Cascade R-CNN (ViT-B) [3]	RGB	33.3	69.3	26.2	51.7	90.3	54.7
DDQ-DETR [80]	RGB	30.9	64.9	24.5	46.7	86.1	45.8
GAFF [74]	RGB+IR	37.4	74.6	31.3	55.8	94.0	60.2
ProbEn [7]	RGB+IR	37.9	75.5	31.8	51.5	93.4	50.2
CSAA [4]	RGB+IR	41.3	79.2	37.4	59.2	94.3	66.6
ICAFusion [45]	RGB+IR	41.4	79.2	36.9	-	-	-
RSDet [83]	RGB+IR	43.8	83.9	40.1	61.3	95.8	70.4
UniRGB-IR (Ours)	RGB+IR	44.1	81.4	40.2	63.2	96.1	72.2

3.3 Supplementary Feature Injector

To adaptively introduce the contextual multi-scale features without altering the ViT structure, we propose a supplementary feature injector (SFI) module as shown in Figure 4. Since the sequence lengths of contextual multi-scale features F_{mfp} and ViT features F_{vit}^i are different, to address this, we employ sparse attention (eg. Pale Attention [62] and Deformable Attention [89]) to dynamically sample supplementary features from each scale. Specifically, we utilize the ViT features $F_{vit}^i \in \mathbb{R}^{\frac{HW}{16^2} \times D}$ as the query, and the contextual multi-scale features $F_{mfp} \in \mathbb{R}^{(\frac{HW}{8^2} + \frac{HW}{16^2} + \frac{HW}{32^2}) \times D}$ as the key and value, which can be represented as:

$$\tilde{F}_{sfi}^i = Attention(LN(F_{vit}^i), LN(F_{mfp})), \quad (2)$$

where $Attention(\cdot)$ is the sparse attention and $LN(\cdot)$ is LayerNorm [1], which aims to reduce modality differences during training. Furthermore, we adopt progressive injection to introduce contextual multi-scale features, which can balance the foundation model features and the injected features F_{sfi}^i . Thus, a gating network is explored to predict the fusion weight z to gate F_{sfi}^{i-1} and \tilde{F}_{sfi}^i for dynamic fusion. Specifically, we concatenate the two features F_{sfi}^{i-1} and \tilde{F}_{sfi}^i and feed it into linear layer to predict the weight z . Then, z and $1-z$ are used to fuse F_{sfi}^{i-1} and \tilde{F}_{sfi}^i features respectively. The final output features F_{sfi}^i of SFI module can be formulated as:

$$F_{sfi}^i = \begin{cases} \tilde{F}_{sfi}^i, & i = 1 \\ (1-z) * \tilde{F}_{sfi}^i + z * F_{sfi}^{i-1}, & i = 2 \dots N \end{cases} \quad (3)$$

3.4 Adapter Tuning Paradigm

To fully inherit the prior knowledge of the ViT pre-trained on large-scale datasets, we explore the adapter tuning paradigm instead of the full fine-tuning manner. For the dataset $D = \{(x_j, gt_j)\}_{j=1}^M$ of

the different semantic tasks, full fine-tuning process calculates the loss between the prediction and the ground truth, which can be formulated as:

$$\mathcal{L}(D, \theta) = \sum_{j=1}^M \text{loss}(F_{\theta}(x_j), gt_j), \quad (4)$$

where loss represents the loss function and F_{θ} denotes the entire network parameterized by θ . Afterwards, θ is optimized through the formula:

$$\theta \leftarrow \arg \min_{\theta} \mathcal{L}(D, \theta). \quad (5)$$

However, in our adapter tuning paradigm, the parameter θ consists of two parts, one part is the parameter in the original ViT model θ_V , and the other part is the parameter in our UniRGB-IR θ_A . During training, we freeze the parameter θ_V and only optimize the parameter θ_A . Thus, the loss function and optimization of our a can be represented as:

$$\mathcal{L}(D, \theta_V, \theta_A) = \sum_{j=1}^M \text{loss}(F_{\theta_V, \theta_A}(x_j), gt_j), \quad (6)$$

$$\theta_A \leftarrow \arg \min_{\theta_A} \mathcal{L}(D, \theta_V, \theta_A). \quad (7)$$

4 Experiments

To evaluate the effectiveness of our UniRGB-IR, we utilize the ViT-Base model (pre-trained on COCO [34] dataset) as the foundation model and utilize this framework to perform RGB-IR semantic tasks. During training, we freeze the ViT-Base model and only optimize the MFP and SFI modules. We evaluate and compare our method with various competitive models, including CNN-based and Transformer-based models. Besides, our evaluation spans various tasks, including RGB-IR object detection on FLIR [73], LLVIP [23], and KAIST [22] datasets, RGB-IR semantic segmentation on PST900

Table 2: RGB-IR pedestrian detection results (MR^{-2} , in%) under ‘All-dataset’ settings of different pedestrian distances, occlusion levels, and light conditions (Day and Night) on the KAIST dataset. The best and second results are highlighted in red and blue.

Methods	Near	Medium	Far	None	Partial	Heavy	Day	Night	All
ACF [22]	28.74	53.67	88.20	62.94	81.40	88.08	64.31	75.06	67.74
Halfway Fusion [35]	8.13	30.34	75.70	43.13	65.21	74.36	47.58	52.35	49.18
FusionRPN+BF [25]	0.04	30.87	88.86	47.45	56.10	72.20	52.33	51.09	51.70
IAF R-CNN [27]	0.96	25.54	77.84	40.17	48.40	69.76	42.46	47.70	44.23
IATDNN+IASS [13]	0.04	28.55	83.42	45.43	46.25	64.57	49.02	49.37	48.96
CIAN [76]	3.71	19.04	55.82	30.31	41.57	62.48	36.02	32.38	35.53
MSDS-R-CNN [26]	1.29	16.19	63.73	29.86	38.71	63.37	32.06	38.83	34.15
AR-CNN [78]	0.00	16.08	69.00	31.40	38.63	55.73	34.36	36.12	34.95
MBNet [85]	0.00	16.07	55.99	27.74	35.43	59.14	32.37	30.95	31.87
TSFADet [71]	0.00	15.99	50.71	25.63	37.29	65.67	31.76	27.44	30.74
CMPD [30]	0.00	12.99	51.22	24.04	33.88	59.37	28.30	30.56	28.98
CAGTDet [70]	0.00	14.00	49.40	24.48	33.20	59.35	28.79	27.73	28.96
C ² Former [72]	0.00	13.71	48.14	23.91	32.84	57.81	28.48	26.67	28.39
UniRGB-IR (Ours)	0.00	13.44	38.21	20.26	31.67	55.03	25.93	23.95	25.21

Table 3: RGB-IR semantic segmentation on the PST900 dataset. The best results are highlighted in red and the second-best are highlighted in blue. “-” indicates that the authors do not provide the corresponding results.

Methods	Background		Fire-Exting.		Backpack		Hand-Drill		Survivor		mAcc	mIoU
	Acc	IoU	Acc	IoU	Acc	IoU	Acc	IoU	Acc	IoU		
MFNet [15]	99.9	98.7	71.8	67.4	52.8	52.4	46.7	39.3	18.8	18.9	58.0	55.3
RTFNet [49]	99.9	99.0	78.6	54.8	62.5	60.8	76.7	61.0	65.2	62.5	76.6	67.6
CCNet [21]	99.6	98.7	88.1	73.8	76.0	73.0	54.1	51.0	49.5	33.5	73.46	66.0
ACNet [20]	99.8	99.3	84.9	60.0	85.6	83.2	53.6	51.5	69.1	65.2	78.7	71.8
PSTNet [47]	-	98.9	-	70.1	-	69.2	-	53.6	-	50.0	-	68.4
FDCNet [82]	99.7	99.2	91.8	71.5	77.5	72.2	82.5	70.4	78.4	72.4	86.0	77.1
CCFFNet [63]	99.9	99.4	87.0	79.3	80.2	77.8	88.3	77.4	77.9	73.4	86.7	81.5
RSFNet [29]	-	99.4	-	75.4	-	84.9	-	72.9	-	70.1	-	80.5
MMDRNet [32]	99.5	98.9	77.9	52.4	79.1	71.1	77.1	40.6	69.8	62.3	81.3	68.7
SGFNet [59]	99.8	99.4	89.4	75.6	90.4	85.4	94.0	76.7	82.7	76.7	91.2	82.8
MDRNet [81]	99.3	99.1	90.2	63.0	93.1	76.3	86.6	63.5	85.6	71.3	91.0	74.6
KDSNet [86]	99.8	99.4	92.0	82.3	83.2	81.2	86.1	71.3	72.6	70.5	86.8	80.9
UniRGB-IR (Ours)	99.7	99.5	97.0	72.0	93.3	87.7	95.5	78.0	86.1	77.8	94.3	82.8

[47] and MFNet [15] (see supplementary materials) datasets and RGB-IR salient object detection on VT821 [57], VT1000 [54] and VT5000 [52]. Furthermore, ablation experiments on the designed modules and qualitative experiments are also conducted to verify that the UniRGB-IR framework can be leveraged as a unified framework to efficiently introduce RGB-IR features into the foundation model to achieve superior performance.

4.1 RGB-IR Object Detection

Datasets. Our object detection experiments are based on the three paired RGB and IR object detection datasets. FLIR [73] is a paired visible and infrared object detection dataset, including daytime and night scenes, which has 4,129 aligned RGB-IR image pairs for training and 1,013 for testing. For LLVIP [23] dataset, it contains 15,488 aligned RGB-IR image pairs, of which 12,025 images are used for training and 3,463 images for testing. As for KAIST [22] dataset,

it is a aligned multispectral pedestrian detection dataset, in which 8,963 and 2,252 image pairs are utilized for training and testing.

Metrics. For FLIR and LLVIP datasets, we employ mean Average Precision (mAP) to evaluate the detection performance. As for KAIST dataset, we use log-average miss rate MR over the false positive per image (FPPI) with the range of $[10^{-2}, 10^0]$ to evaluate the pedestrian detection performance.

Settings. All the experiments are conducted with NVIDIA GeForce RTX 3090 GPUs. We implement our framework on the MMDetection library and use the Cascade R-CNN [3] as the basic framework to perform RGB-IR object detection. The detector is trained with an initial learning rate of 2×10^{-4} for 48 epochs. The batch size is set to 16, and the AdamW [41] optimizer is employed with a weight decay of 0.1. Horizontal flipping is also used for data augmentation.

Results on FLIR and LLVIP datasets. We compare our method with five common mono-modality methods and four competitive multi-modality methods. As shown in Table 1, it can be seen that

Table 4: RGB-IR salient object detection on VT821, VT1000 and VT5000 datasets. * represents RGB-D SOD transformed into RGB-T SOD. The best results are highlighted in red and the second-best are highlighted in blue.

Model	VT821				VT1000				VT5000			
	S \uparrow	adpE \uparrow	adpF \uparrow	MAE \downarrow	S \uparrow	adpE \uparrow	adpF \uparrow	MAE \downarrow	S \uparrow	adpE \uparrow	adpF \uparrow	MAE \downarrow
MMCI* [6]	0.763	0.784	0.618	0.087	0.886	0.892	0.803	0.039	0.827	0.859	0.714	0.055
TANet* [5]	0.818	0.852	0.717	0.052	0.902	0.912	0.838	0.030	0.847	0.883	0.754	0.047
S2MA* [37]	0.811	0.813	0.709	0.098	0.918	0.912	0.848	0.029	0.853	0.864	0.743	0.053
JLDCF* [12]	0.839	0.830	0.726	0.076	0.912	0.899	0.829	0.030	0.861	0.860	0.739	0.050
MTMR [57]	0.725	0.815	0.662	0.109	0.706	0.836	0.715	0.119	0.680	0.795	0.595	0.114
M3S-NIR [53]	0.723	0.859	0.734	0.140	0.726	0.827	0.717	0.145	0.652	0.780	0.575	0.168
SGDL [54]	0.765	0.847	0.731	0.085	0.787	0.856	0.764	0.090	0.750	0.824	0.672	0.089
FMSF [79]	0.760	0.796	0.640	0.080	0.873	0.899	0.823	0.037	0.814	0.864	0.734	0.055
MIDD [51]	0.871	0.895	0.803	0.063	0.915	0.933	0.880	0.027	0.868	0.896	0.799	0.043
ADF [52]	0.810	0.842	0.717	0.077	0.910	0.921	0.847	0.034	0.864	0.891	0.778	0.048
LSNet [88]	0.877	0.911	0.827	0.070	0.924	0.936	0.887	0.022	0.876	0.916	0.827	0.036
UniTR [14]	0.873	0.892	0.827	0.033	0.929	0.941	0.885	0.019	0.883	0.926	0.839	0.032
UniRGB-IR (Ours)	0.881	0.895	0.806	0.039	0.939	0.943	0.894	0.018	0.906	0.935	0.849	0.027

most of the multi-modality detectors are even worse than mono-modality detectors (eg. Cascade R-CNN in IR modality). Since RGB features interfere with infrared feature under limited illumination conditions, it has a negative impact on the fused features utilized for object detection tasks. However, our UniRGB-IR can effectively solve this problem through the SFI module, enabling the detector to achieve better classification and localization processes.

Results on KAIST dataset. The quantitative results of the different methods on the KAIST dataset are shown in Table 2. The experiments are conducted under ‘All-dataset’ settings [22]. We compare our UniRGB-IR with thirteen multi-modal object detection methods. Our model achieves the best performance on the ‘All’, ‘Day’, and ‘Night’ conditions and the other four of five subsets (‘Near’, ‘Far’, ‘None’, ‘Partial’ and ‘Heavy’), and rank second in the ‘Medium’ subset. Furthermore, our detector surpasses the previous best competitor C²Former by 3.18% on the ‘All’ condition, which indicates UniRGB-IR is robust to the complex scenes.

4.2 RGB-IR Semantic Segmentation

Datasets. Our semantic segmentation experiments are performed on the two public RGB-IR semantic segmentation datasets: PST900 [47] and MFNet [15] (see supplementary materials). The PST900 dataset is divided into 597 pairs for training and 288 pairs for testing, containing five categories (background, fire extinguisher, backpack, hand drill, and survivor). The dataset is divided into three parts: training, verification and testing according to the ratio of 2:1:1.

Metrics. Two metrics are utilized to evaluate the performance of semantic segmentation, namely mean accuracy (mAcc) and mean intersection over union (mIoU). Both metrics are calculated by averaging the ratios of the intersection and union of all categories.

Settings. Similarly, as the RGB-IR object detection task, we incorporate our method into the SETR [84] basic framework and implement it on the MMSegmentation library. The fine-tuning process spins a total of 10K iterations with an initial learning rate of 0.01. We employ the SGD optimizer and set the batch size to 16.

Results. The quantitative results of the different RGB-IR segmentation methods on the PST900 dataset are shown in Table 3. The

Table 5: Ablation studies of key components on the FLIR and PST900 datasets. The best results are highlighted in bold.

MFP	SFI	FLIR			PST900	
		mAP	mAP ₅₀	mAP ₇₅	mAcc	mIoU
		39.6	76.3	35.9	90.1	77.5
✓		41.2	77.9	36.5	91.7	78.8
✓	✓	44.1	81.4	40.2	94.3	82.8

comparison results show that our model significantly outperforms other methods. Specifically, our model obtains the best performance in terms of both the mACC and mIoU. Besides, our model performs competitive performance in the Backpack, Hand-Drill and Survivor, outperforming the second-best methods by 2.3%, 0.6% and 1.1% IoU, which strongly demonstrates the effectiveness of our UniRGB-IR.

4.3 RGB-IR Salient Object Detection

Datasets. Our salient object detection (SOD) experiments are performed on the three public datasets: VT821 [57], VT1000 [54] and VT5000 [52]. The VT821 dataset includes 821 registered RGB and IR images. The VT1000 dataset contains 1000 registered RGB-IR images with simple scenes and aligned images. The VT5000 dataset is a recent large-scale RGB-IR dataset, including a full-day scene under various limited light conditions. As usual in [52], we utilize 2500 image pairs in the VT5000 dataset as the training dataset, and the remaining image pairs along with the image pairs from the VT821 and VT1000 datasets are used as the test datasets.

Metrics. Four metrics are utilized to evaluate the performance of salient object detection namely F-measure (adpF \uparrow), E-Measure (adpE \uparrow), S-Measure (S \uparrow) and Mean absolute error (MAE \downarrow). \uparrow and \downarrow denote the higher the better and the lower the better, respectively.

Settings. As same as the RGB-IR semantic segmentation task, we incorporate our method into the SETR basic framework and also implement it on the MMSegmentation library. The fine-tuning process spins a total of 10K iterations with an initial learning rate

Table 6: Ablation of adding SFI module to different stages.

Different Stages with SFI module				mAP	mAP ₅₀	mAP ₇₅
Stage 1	Stage 2	Stage 3	Stage 4			
✓				41.7	80.0	37.2
✓	✓			43.3	81.6	39.7
✓	✓	✓		44.1	81.4	40.2
✓	✓	✓	✓	42.7	79.9	38.2

Table 7: Ablation of the different attention mechanisms.

Attention Mechanism	Complexity	mAP	mAP ₅₀	mAP ₇₅
Global Attention [56]	Quadratic	36.1	72.8	30.6
Pale Attention [62]	Linear	31.6	68.4	24.6
Deformable Attention [89]	Linear	44.1	81.4	40.2

of 0.01. We use the SGD optimizer and set the batch size to 64. For convenience, all input images are resized to 224×224 for testing. **Results.** Table 4 reports the quantitative comparison results. As can be seen from Table 4, our UniRGB-IR outperforms SOTA methods both on VT1000 and VT5000 datasets in all evaluation metrics. Specifically, the S , $adpE$, $adpF$ and MAE metrics of our UniRGB-IR achieve 0.906, 0.935, 0.849 and 0.027 on VT5000, all of which are higher than the previous competitor UniT [14]. These remarkable results clearly indicate that the saliency maps predicted by UniRGB-IR are close to the corresponding ground-truths.

4.4 Ablation Study

Ablation for components. To investigate the contribution of the SFI and MFP modules, we gradually add each module to the baseline model as shown in Table 5. We stack RGB and IR images and feed them into the Cascade R-CNN detector and SETR framework (ViT-Adapter backbone) for full fine-tuning on the corresponding tasks, which are considered as our baseline models. Then, we freeze the ViT model and introduce the MFP module to extract contextual multi-scale features (element-wise addition), which results in 1.6% mAP and 1.3% mIoU improvements. Finally, we replace the element-wise addition operation with the SFI module and further improve the mAP and mIoU metrics by 2.9% and 4.0% respectively, which achieve the best performance on both datasets.

SFI module at different stages. We add the SFI module to the ViT pre-trained model at the beginning of different stages. From Table 6, we can find that by adding the SFI module at the first stage, the detector achieves 41.7% mAP on FLIR dataset. After adding the SFI module in the second and third stages, the performance further improved by about 2% and 3% mAP, respectively. However, continuing to add it to the final stage will reduce the detection performance while also increasing computational overhead. Therefore, we add the SFI module from the first stage to the third stage of ViT model. **Attention type in SFI module.** Since the attention mechanism in our SFI module is replaceable, we adopt three popular attention mechanisms in our UniRGB-IR to discuss their impact on model performance. As shown in Table 7, the detector achieves the best performance with linear complexity by utilizing deformable attention. Thus, the deformable attention is more suitable for our

framework and utilized as the default configuration. It is worth noting that it can be replaced by other attention mechanisms to further achieve superior performance.

4.5 Visualization Analysis

Intermediate results. To illustrate the effectiveness of the SFI module, we visualize the intermediate results on the FLIR dataset. From F_{mfp} and F_{sfi} in Figure 5, we can find that the foreground objects in the F_{sfi} become salient through the SFI module. Furthermore, we also visualize the tSNE maps of $F_{mfp}-F_{vit}$ and $F_{sfi}-F_{vit}$ respectively. After using the SFI module, the distribution of injected features F_{sfi} is more concentrated than the distribution of ViT features F_{vit} , indicating that the required richer RGB-IR features can be well supplemented into the ViT model through the SFI module. **Training efficiency.** We further plot the mAP curves for each epoch of UniRGB-IR with different training paradigm to demonstrate the efficiency of UniRGB-IR, as shown in Figure 6. During the training process, all hyperparameters of the two models are the same. From Figure 6, we can find that the convergence speed of the adapter tuning paradigm surpasses that of the full fine-tuning strategy. Moreover, by utilizing the adapter tuning paradigm, our UniRGB-IR achieves superior performance with a smaller number of trainable parameters (about 10% of the full fine-tuning model). The above results verify the efficiency of our method.

5 Conclusion

In this paper, we proposed an efficient and scalable framework (named UniRGB-IR) for RGB-IR semantic tasks. The framework contains a Multi-modal Feature Pool module and a Supplementary Feature Injector module. The former extracts contextual multi-scale features from two modality images, and the latter adaptively injects the features into the transformer model. These two modules can be efficiently optimized to complement the pre-trained foundation model with richer RGB-IR features. To evaluate the effectiveness of our method, we incorporated the ViT-Base model into the framework as the pre-trained foundation model and performed various RGB-IR semantic tasks. Extensive experiments verify that our UniRGB-IR can be effectively leveraged as a unified framework for RGB-IR downstream tasks. We believe that our method can be applied to more multi-modal real-world applications.

References

- [1] Jimmy Lei Ba, Jamie Ryan Kiros, and Geoffrey E Hinton. 2016. Layer normalization. *arXiv preprint arXiv:1607.06450* (2016).
- [2] LI Bo, XIE Xiaoyang, WEI Xingxing, and TANG Wenting. 2021. Ship detection and classification from optical remote sensing images: A survey. *Chinese Journal of Aeronautics* 34, 3 (2021), 145–163.
- [3] Zhaowei Cai and Nuno Vasconcelos. 2018. Cascade r-cnn: Delving into high quality object detection. In *Proceedings of the IEEE conference on computer vision and pattern recognition*. 6154–6162.
- [4] Yue Cao, Junchi Bin, Jozsef Hamari, Erik Blasch, and Zheng Liu. 2023. Multimodal Object Detection by Channel Switching and Spatial Attention. In *Proceedings of the IEEE/CVF Conference on Computer Vision and Pattern Recognition Workshops*. 403–411.
- [5] Hao Chen and Youfu Li. 2019. Three-stream attention-aware network for RGB-D salient object detection. *TIP* 28, 6 (2019), 2825–2835.
- [6] Hao Chen, Youfu Li, and Dan Su. 2019. Multi-modal fusion network with multi-scale multi-path and cross-modal interactions for RGB-D salient object detection. *Pattern Recognition* 86 (2019), 376–385.
- [7] Yi-Ting Chen, Jinghao Shi, Zelin Ye, Christoph Mertz, Deva Ramanan, and Shu Kong. 2022. Multimodal object detection via probabilistic ensembling. In *European*

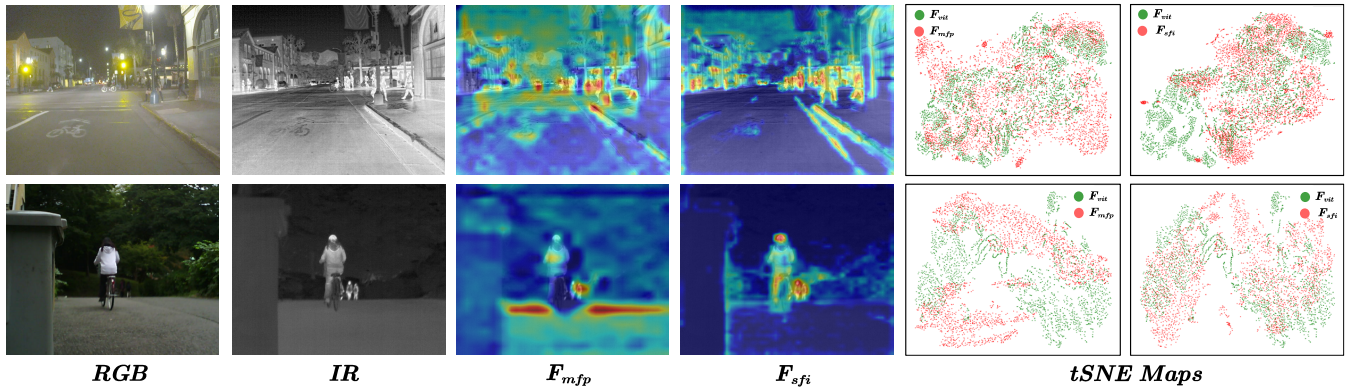


Figure 5: Visualization of intermediate results. The F_{mfp} and F_{sfi} features from the first stage are visualized in the third and fourth columns. The tSNE visualizations are also shown in the last two columns.

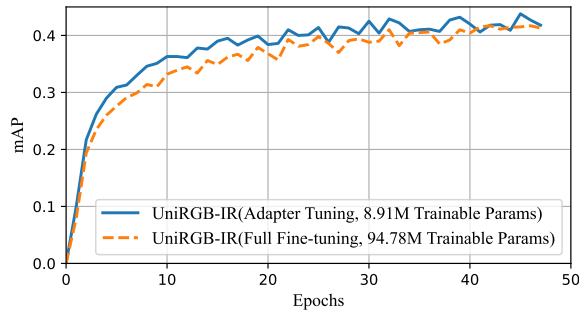


Figure 6: Training efficiency analysis on the FLIR dataset.

Conference on Computer Vision. Springer, 139–158.

[8] Zhe Chen, Yuchen Duan, Wenhai Wang, Junjun He, Tong Lu, Jifeng Dai, and Yu Qiao. 2022. Vision transformer adapter for dense predictions. *arXiv preprint arXiv:2205.08534* (2022).

[9] Jia Deng, Wei Dong, Richard Socher, Li-Jia Li, Kai Li, and Li Fei-Fei. 2009. Imagenet: A large-scale hierarchical image database. In *2009 IEEE conference on computer vision and pattern recognition*. Ieee, 248–255.

[10] Alexey Dosovitskiy, Lucas Beyer, Alexander Kolesnikov, Dirk Weissenborn, Xi-aohua Zhai, Thomas Unterthiner, Mostafa Dehghani, Matthias Minderer, Georg Heigold, Sylvain Gelly, et al. 2020. An image is worth 16x16 words: Transformers for image recognition at scale. *arXiv preprint arXiv:2010.11929* (2020).

[11] Haoqi Fan, Bo Xiong, Karttikeya Mangalam, Yanghao Li, Zhicheng Yan, Jitendra Malik, and Christoph Feichtenhofer. 2021. Multiscale vision transformers. In *Proceedings of the IEEE/CVF international conference on computer vision*. 6824–6835.

[12] Keren Fu, Deng-Ping Fan, Ge-Peng Ji, Qijun Zhao, Jianbing Shen, and Ce Zhu. 2021. Siamese network for RGB-D salient object detection and beyond. *TPAMI* 44, 9 (2021), 5541–5559.

[13] Dayan Guan, Yanpeng Cao, Jiangxin Yang, Yanlong Cao, and Michael Ying Yang. 2019. Fusion of multispectral data through illumination-aware deep neural networks for pedestrian detection. *Information Fusion* 50 (2019), 148–157.

[14] Ruohao Guo, Xianghua Ying, Yanyu Qi, and Liao Qu. 2024. UniTR: A unified transformer-based framework for co-object and multi-modal saliency detection. *IEEE transactions on multimedia* (2024).

[15] Qishen Ha, Kohei Watanabe, Takumi Karasawa, Yoshitaka Ushiku, and Tatsuya Harada. 2017. MFNet: Towards real-time semantic segmentation for autonomous vehicles with multi-spectral scenes. In *2017 IEEE/RSJ International Conference on Intelligent Robots and Systems (IROS)*. IEEE, 5108–5115.

[16] Kaiming He, Xiangyu Zhang, Shaoqing Ren, and Jian Sun. 2016. Deep residual learning for image recognition. In *Proceedings of the IEEE conference on computer vision and pattern recognition*. 770–778.

[17] Zewei He, Yanpeng Cao, Lei Du, Baohei Xu, Jiangxin Yang, Yanlong Cao, Siliang Tang, and Yueting Zhuang. 2019. MRFN: Multi-receptive-field network for fast and accurate single image super-resolution. *IEEE Transactions on Multimedia* 22,

4 (2019), 1042–1054.

[18] Neil Houlsby, Andrei Giurgiu, Stanislaw Jastrzebski, Bruna Morrone, Quentin De Laroussilhe, Andrea Gesmundo, Mona Attariyan, and Sylvain Gelly. 2019. Parameter-efficient transfer learning for NLP. In *International conference on machine learning*. PMLR, 2790–2799.

[19] Jie Hu, Li Shen, and Gang Sun. 2018. Squeeze-and-excitation networks. In *Proceedings of the IEEE conference on computer vision and pattern recognition*. 7132–7141.

[20] Xinxin Hu, Kailun Yang, Lei Fei, and Kaiwei Wang. 2019. Acnet: Attention based network to exploit complementary features for rgb-d semantic segmentation. In *2019 IEEE International conference on image processing (ICIP)*. IEEE, 1440–1444.

[21] Zilong Huang, Xinggang Wang, Lichao Huang, Chang Huang, Yunchao Wei, and Wenyu Liu. 2019. Ccnet: Criss-cross attention for semantic segmentation. In *Proceedings of the IEEE/CVF international conference on computer vision*. 603–612.

[22] Soonmin Hwang, Jaesik Park, Namil Kim, Yukyung Choi, and In So Kweon. 2015. Multispectral pedestrian detection: Benchmark dataset and baseline. In *Proceedings of the IEEE conference on computer vision and pattern recognition*. 1037–1045.

[23] Xinyu Jia, Chuang Zhu, Minzhen Li, Wenqi Tang, and Wenli Zhou. 2021. LLVIP: A visible-infrared paired dataset for low-light vision. In *Proceedings of the IEEE/CVF international conference on computer vision*. 3496–3504.

[24] Asifullah Khan, Anabia Sohail, Umme Zahoor, and Aqsa Saeed Qureshi. 2020. A survey of the recent architectures of deep convolutional neural networks. *Artificial intelligence review* 53 (2020), 5455–5516.

[25] Daniel Konig, Michael Adam, Christian Jarvers, Georg Layher, Heiko Neumann, and Michael Teutsch. 2017. Fully convolutional region proposal networks for multispectral person detection. In *Proceedings of the IEEE conference on computer vision and pattern recognition workshops*. 49–56.

[26] Chengyang Li, Dan Song, Ruofeng Tong, and Min Tang. 2018. Multispectral Pedestrian Detection via Simultaneous Detection and Segmentation. In *British Machine Vision Conference (BMVC)*.

[27] Chengyang Li, Dan Song, Ruofeng Tong, and Min Tang. 2019. Illumination-aware faster R-CNN for robust multispectral pedestrian detection. *Pattern Recognition* 85 (2019), 161–171.

[28] Feng Li, Hao Zhang, Huaizhe Xu, Shilong Liu, Lei Zhang, Lionel M Ni, and Heung-Yeung Shum. 2023. Mask dino: Towards a unified transformer-based framework for object detection and segmentation. In *Proceedings of the IEEE/CVF Conference on Computer Vision and Pattern Recognition*. 3041–3050.

[29] Ping Li, Junjie Chen, Binbin Lin, and Xianghua Xu. 2023. Residual spatial fusion network for rgb-thermal semantic segmentation. *arXiv preprint arXiv:2306.10364* (2023).

[30] Qing Li, Changqing Zhang, Qinghua Hu, Huazhu Fu, and Pengfei Zhu. 2022. Confidence-aware fusion using dempster-shafer theory for multispectral pedestrian detection. *IEEE Transactions on Multimedia* (2022).

[31] Yanghao Li, Hanzi Mao, Ross Girshick, and Kaiming He. 2022. Exploring plain vision transformer backbones for object detection. In *European Conference on Computer Vision*. Springer, 280–296.

[32] Wenli Liang, Yuanjian Yang, Fangyu Li, Xi Long, and Caifeng Shan. 2023. Mask-guided modality difference reduction network for RGB-T semantic segmentation. *Neurocomputing* 523 (2023), 9–17.

[33] Tsung-Yi Lin, Priya Goyal, Ross Girshick, Kaiming He, and Piotr Dollár. 2017. Focal loss for dense object detection. In *Proceedings of the IEEE international conference on computer vision*. 2980–2988.

- [34] Tsung-Yi Lin, Michael Maire, Serge Belongie, James Hays, Pietro Perona, Deva Ramanan, Piotr Dollár, and C Lawrence Zitnick. 2014. Microsoft coco: Common objects in context. In *Computer Vision—ECCV 2014: 13th European Conference, Zurich, Switzerland, September 6–12, 2014, Proceedings, Part V 13*. Springer, 740–755.
- [35] Jingjing Liu, Shaoting Zhang, Shu Wang, and Dimitris N Metaxas. 2016. Multispectral deep neural networks for pedestrian detection. *arXiv preprint arXiv:1611.02644* (2016).
- [36] Lingbo Liu, Jiaqi Chen, Hefeng Wu, Guanbin Li, Chenglong Li, and Liang Lin. 2021. Cross-modal collaborative representation learning and a large-scale rgbt benchmark for crowd counting. In *Proceedings of the IEEE/CVF conference on computer vision and pattern recognition*. 4823–4833.
- [37] Nian Liu, Ni Zhang, and Junwei Han. 2020. Learning selective self-mutual attention for RGB-D saliency detection. In *CVPR*. 13756–13765.
- [38] Wei Liu, Dragomir Anguelov, Dumitru Erhan, Christian Szegedy, Scott Reed, Cheng-Yang Fu, and Alexander C Berg. 2016. Ssd: Single shot multibox detector. In *Computer Vision—ECCV 2016: 14th European Conference, Amsterdam, The Netherlands, October 11–14, 2016, Proceedings, Part I 14*. Springer, 21–37.
- [39] Ze Liu, Yutong Lin, Yue Cao, Han Hu, Yixuan Wei, Zheng Zhang, Stephen Lin, and Baining Guo. 2021. Swin transformer: Hierarchical vision transformer using shifted windows. In *Proceedings of the IEEE/CVF international conference on computer vision*. 10012–10022.
- [40] Zhengyi Liu, Yacheng Tan, Qian He, and Yun Xiao. 2021. SwinNet: Swin transformer drives edge-aware RGB-D and RGB-T salient object detection. *IEEE Transactions on Circuits and Systems for Video Technology* 32, 7 (2021), 4486–4497.
- [41] Ilya Loshchilov and Frank Hutter. 2017. Decoupled weight decay regularization. *arXiv preprint arXiv:1711.05101* (2017).
- [42] Youwei Pang, Xiaoyi Zhao, Libe Zhang, and Huchuan Lu. 2023. Caver: Cross-modal view-mixed transformer for bi-modal salient object detection. *IEEE Transactions on Image Processing* 32 (2023), 892–904.
- [43] Joonhyung Park, Hyunjin Seo, and Eunho Yang. 2023. PC-Adapter: Topology-Aware Adapter for Efficient Domain Adaption on Point Clouds with Rectified Pseudo-label. In *Proceedings of the IEEE/CVF International Conference on Computer Vision*. 11530–11540.
- [44] Shaoping Ren, Kaiming He, Ross Girshick, and Jian Sun. 2015. Faster r-cnn: Towards real-time object detection with region proposal networks. *Advances in neural information processing systems* 28 (2015).
- [45] Jifeng Shen, Yifei Chen, Yue Liu, Xin Zuo, Heng Fan, and Wankou Yang. 2024. ICAFusion: Iterative cross-attention guided feature fusion for multispectral object detection. *Pattern Recognition* 145 (2024), 109913.
- [46] Yifeng Shi, Feng Lv, Xinliang Wang, Chunlong Xia, Shaojie Li, Shujie Yang, Teng Xi, and Gang Zhang. 2023. Open-transmind: A new baseline and benchmark for 1st foundation model challenge of intelligent transportation. In *Proceedings of the IEEE/CVF Conference on Computer Vision and Pattern Recognition*. 6327–6334.
- [47] Shreyas S Shivakumar, Neil Rodrigues, Alex Zhou, Ian D Miller, Vijay Kumar, and Camillo J Taylor. 2020. Pst900: Rgb-thermal calibration, dataset and segmentation network. In *2020 IEEE international conference on robotics and automation (ICRA)*. IEEE, 9441–9447.
- [48] Asa Cooper Stickland and Iain Murray. 2019. Bert and pals: Projected attention layers for efficient adaptation in multi-task learning. In *International Conference on Machine Learning*. PMLR, 5986–5995.
- [49] Yuxiang Sun, Weixun Zuo, and Ming Liu. 2019. Rtfnet: Rgb-thermal fusion network for semantic segmentation of urban scenes. *IEEE Robotics and Automation Letters* 4, 3 (2019), 2576–2583.
- [50] Yi-Lin Sung, Jaemin Cho, and Mohit Bansal. 2022. Vl-adapter: Parameter-efficient transfer learning for vision-and-language tasks. In *Proceedings of the IEEE/CVF Conference on Computer Vision and Pattern Recognition*. 5227–5237.
- [51] Zhengzheng Tu, Zhun Li, Chenglong Li, Yang Lang, and Jin Tang. 2021. Multi-interactive dual-decoder for RGB-thermal salient object detection. *IEEE Transactions on Image Processing* 30 (2021), 5678–5691.
- [52] Zhengzheng Tu, Yan Ma, Zhun Li, Chenglong Li, Jieming Xu, and Yongtao Liu. 2022. RGBT salient object detection: A large-scale dataset and benchmark. *TMM* (2022).
- [53] Zhengzheng Tu, Tian Xia, Chenglong Li, Yijuan Lu, and Jin Tang. 2019. M3S-NIR: Multi-modal multi-scale noise-insensitive ranking for RGB-T saliency detection. In *MIPR*. IEEE, 141–146.
- [54] Zhengzheng Tu, Tian Xia, Chenglong Li, Xiaoxiao Wang, Yan Ma, and Jin Tang. 2019. RGB-T image saliency detection via collaborative graph learning. *TMM* 22, 1 (2019), 160–173.
- [55] Uddeshya Upadhyay, Shyamgopal Karthik, Massimiliano Mancini, and Zeynep Akata. 2023. Problm: Probabilistic adapter for frozen vision-language models. In *Proceedings of the IEEE/CVF International Conference on Computer Vision*. 1899–1910.
- [56] Ashish Vaswani, Noam Shazeer, Niki Parmar, Jakob Uszkoreit, Llion Jones, Aidan N Gomez, Łukasz Kaiser, and Illia Polosukhin. 2017. Attention is all you need. *Advances in neural information processing systems* 30 (2017).
- [57] Guizhao Wang, Chenglong Li, Yunpeng Ma, Aihua Zheng, Jin Tang, and Bin Luo. 2018. RGB-T saliency detection benchmark: Dataset, baselines, analysis and a novel approach. In *IGTA*. Springer, 359–369.
- [58] Wenhui Wang, Enze Xie, Xiang Li, Deng-Ping Fan, Kaitao Song, Ding Liang, Tong Lu, Ping Luo, and Ling Shao. 2021. Pyramid vision transformer: A versatile backbone for dense prediction without convolutions. In *Proceedings of the IEEE/CVF international conference on computer vision*. 568–578.
- [59] Yike Wang, Gongyang Li, and Zhi Liu. 2023. Sgfnnet: semantic-guided fusion network for rgb-thermal semantic segmentation. *IEEE Transactions on Circuits and Systems for Video Technology* (2023).
- [60] Zhaokai Wang, Xizhou Zhu, Xue Yang, Gen Luo, Hao Li, Changyao Tian, Wenhan Dou, Junqi Ge, Lewei Lu, Yu Qiao, et al. 2025. Parameter-Inverted Image Pyramid Networks for Visual Perception and Multimodal Understanding. *arXiv preprint arXiv:2501.07783* (2025).
- [61] Xingxing Wei, Yao Huang, Yitong Sun, and Jie Yu. 2023. Unified Adversarial Patch for Visible-Infrared Cross-modal Attacks in the Physical World. *IEEE Transactions on Pattern Analysis and Machine Intelligence* (2023).
- [62] Sitong Wu, Tianyi Wu, Haoru Tan, and Guodong Guo. 2022. Pale transformer: A general vision transformer backbone with pale-shaped attention. In *Proceedings of the AAAI Conference on Artificial Intelligence*, Vol. 36. 2731–2739.
- [63] Wei Wu, Tao Chu, and Qiong Liu. 2022. Complementarity-aware cross-modal feature fusion network for RGB-T semantic segmentation. *Pattern Recognition* 131 (2022), 108881.
- [64] Xin Wu, Danfeng Hong, and Jocelyn Chanasot. 2022. UIU-Net: U-Net in U-Net for infrared small object detection. *IEEE Transactions on Image Processing* 32 (2022), 364–376.
- [65] Chunlong Xia, Xinliang Wang, Feng Lv, Xin Hao, and Yifeng Shi. 2024. ViT-CoMer: Vision Transformer with Convolutional Multi-scale Feature Interaction for Dense Predictions. *arXiv preprint arXiv:2403.07392* (2024).
- [66] Dan Xu, Wanli Ouyang, Elisa Ricci, Xiaogang Wang, and Nico Sebe. 2017. Learning cross-modal deep representations for robust pedestrian detection. In *Proceedings of the IEEE conference on computer vision and pattern recognition*. 5363–5371.
- [67] Huanqian Yan, Bo Li, Hong Zhang, and Xingxing Wei. 2022. An anti-jamming and lightweight ship detector designed for spaceborne optical images. *IEEE Journal of Selected Topics in Applied Earth Observations and Remote Sensing* 15 (2022), 4468–4481.
- [68] Dongshuo Yin, Leiyi Hu, Bin Li, Youqun Zhang, and Xue Yang. 2025. 5%–100%: Breaking performance shackles of full fine-tuning on visual recognition tasks. In *Proceedings of the IEEE/CVF Conference on Computer Vision and Pattern Recognition*.
- [69] Dongshuo Yin, Yiran Yang, Zhechao Wang, Hongfeng Yu, Kaiwen Wei, and Xian Sun. 2023. 1% vs 100%: Parameter-efficient low rank adapter for dense predictions. In *Proceedings of the IEEE/CVF Conference on Computer Vision and Pattern Recognition*. 20116–20126.
- [70] Maouxun Yuan, Xiaorong Shi, Nan Wang, Yinyan Wang, and Xingxing Wei. 2024. Improving RGB-infrared object detection with cascade alignment-guided transformer. *Information Fusion* 105 (2024), 102246.
- [71] Maouxun Yuan, Yinyan Wang, and Xingxing Wei. 2022. Translation, scale and rotation: cross-modal alignment meets RGB-infrared vehicle detection. In *European Conference on Computer Vision*. Springer, 509–525.
- [72] Maouxun Yuan and Xingxing Wei. 2024. C2Former: Calibrated and Complementary Transformer for RGB-Infrared Object Detection. *IEEE Transactions on Geoscience and Remote Sensing* (2024), 1–1.
- [73] Heng Zhang, Elisa Fromont, Sébastien Lefevre, and Bruno Avignon. 2020. Multi-spectral fusion for object detection with cyclic fuse-and-refine blocks. In *2020 IEEE International conference on image processing (ICIP)*. IEEE, 276–280.
- [74] Heng Zhang, Elisa Fromont, Sébastien Lefevre, and Bruno Avignon. 2021. Guided attentive feature fusion for multispectral pedestrian detection. In *Proceedings of the IEEE/CVF winter conference on applications of computer vision*. 72–80.
- [75] Jiaming Zhang, Huayao Liu, Kailun Yang, Xinxin Hu, Ruiping Liu, and Rainer Stiefelhagen. 2023. CMX: Cross-modal fusion for RGB-X semantic segmentation with transformers. *IEEE Transactions on Intelligent Transportation Systems* (2023).
- [76] Lu Zhang, Zhiyong Liu, Shifeng Zhang, Xu Yang, Hong Qiao, Kaizhu Huang, and Amir Hussain. 2019. Cross-modality interactive attention network for multispectral pedestrian detection. *Information Fusion* 50 (2019), 20–29.
- [77] Lu Zhang, Zhiyong Liu, Xiangyu Zhu, Zhan Song, Xu Yang, Zhen Lei, and Hong Qiao. 2021. Weakly aligned feature fusion for multimodal object detection. *IEEE Transactions on Neural Networks and Learning Systems* (2021).
- [78] Lu Zhang, Xiangyu Zhu, Xiangyu Chen, Xu Yang, Zhen Lei, and Zhiyong Liu. 2019. Weakly aligned cross-modal learning for multispectral pedestrian detection. In *Proceedings of the IEEE/CVF international conference on computer vision*. 5127–5137.
- [79] Qiang Zhang, Nianchang Huang, Lin Yao, Dingwen Zhang, Caifeng Shan, and Jungong Han. 2019. RGB-T salient object detection via fusing multi-level CNN features. *IEEE Transactions on Image Processing* 29 (2019), 3321–3335.
- [80] Shilong Zhang, Xinjiang Wang, Jiaqi Wang, Jiangmiao Pang, Chengqi Lyu, Wenwei Zhang, Ping Luo, and Kai Chen. 2023. Dense distinct query for end-to-end object detection. In *Proceedings of the IEEE/CVF conference on computer vision and pattern recognition*. 7329–7338.

- [81] Shenlu Zhao, Yichen Liu, Qiang Jiao, Qiang Zhang, and Jungong Han. 2024. Mitigating modality discrepancies for RGB-T semantic segmentation. *IEEE Transactions on Neural Networks and Learning Systems* (2024).
- [82] Shenlu Zhao and Qiang Zhang. 2022. A feature divide-and-conquer network for rgb-t semantic segmentation. *IEEE Transactions on Circuits and Systems for Video Technology* (2022).
- [83] Tianyi Zhao, Maoxun Yuan, and Xingxing Wei. 2024. Removal and Selection: Improving RGB-Infrared Object Detection via Coarse-to-Fine Fusion. *arXiv preprint arXiv:2401.10731* (2024).
- [84] Sixiao Zheng, Jiachen Lu, Hengshuang Zhao, Xiatian Zhu, Zekun Luo, Yabiao Wang, Yanwei Fu, Jianfeng Feng, Tao Xiang, Philip HS Torr, et al. 2021. Rethinking semantic segmentation from a sequence-to-sequence perspective with transformers. In *CVPR*. 6881–6890.
- [85] Kailai Zhou, Linsen Chen, and Xun Cao. 2020. Improving multispectral pedestrian detection by addressing modality imbalance problems. In *Computer Vision–ECCV 2020: 16th European Conference, Glasgow, UK, August 23–28, 2020, Proceedings, Part XVIII 16*. Springer, 787–803.
- [86] Wujie Zhou, Tingting Gong, and Weiqing Yan. 2024. Knowledge distillation segformer-based network for RGB-T semantic segmentation. *IEEE Transactions on Systems, Man, and Cybernetics: Systems* (2024).
- [87] Wujie Zhou, Fan Sun, Qiuping Jiang, Runmin Cong, and Jenq-Neng Hwang. 2023. WaveNet: Wavelet network with knowledge distillation for RGB-T salient object detection. *IEEE Transactions on Image Processing* (2023).
- [88] Wujie Zhou, Yun Zhu, Jingsheng Lei, Rongwang Yang, and Lu Yu. 2023. LSNet: Lightweight spatial boosting network for detecting salient objects in RGB-thermal images. *IEEE Transactions on Image Processing* 32 (2023), 1329–1340.
- [89] Xizhou Zhu, Weijie Su, Lewei Lu, Bin Li, Xiaogang Wang, and Jifeng Dai. 2020. Deformable detr: Deformable transformers for end-to-end object detection. *arXiv preprint arXiv:2010.04159* (2020).
- [90] Xizhou Zhu, Xue Yang, Zhaokai Wang, Hao Li, Wenhan Dou, Junqi Ge, Lewei Lu, Yu Qiao, and Jifeng Dai. 2024. Parameter-inverted image pyramid networks. *Advances in Neural Information Processing Systems* 37 (2024), 132267–132288.